IEEE Access
Multidisciplinary ⋮ Rapid Review ⋮ Open Access Journal

Received September 24, 2019, accepted October 16, 2019, date of publication October 31, 2019,
date of current version December 31, 2019.

Digital Object Identifier 10.1109/ACCESS.2019.2950819

An Intelligent Implementation of Fuzzy Search Based Nonlinear Droop Control Scheme for Multi-Terminal DC Transmission Systems

JIEBEI ZHU[1], (Member, IEEE), FENG LI[1], YINGSHU LIU[1], GRAIN PHILIP ADAM[2], (Member, IEEE), MINGYING LI[3], AND NING SUN[3]

[1]School of Electrical and Information Engineering, Tianjin University, Tianjin 300072, China
[2]Department of Electronic and Electrical Engineering, University of Strathclyde, Glasgow G1 1XQ, U.K.
[3]State Grid Electric Power Research Institute, Nanjing 211106, China

Corresponding author: Feng Li (li_power7044@163.com)

This work was supported in part by the China National Key Research and Development Plan in Transformative Technologies: Intelligent Evolution Mechanism and Design of Distributed Information Energy Systems under Grant 2018YFA070220, in part by the National Natural Science Foundation of China in Research and Development of New Collaborative Virtual Synchronous Generator Scheme Based on DC System Strength under Grant 51977143, and in part by the China State Grid Technology Project: Intrinsic Safety Improvement of AC/DC Power Grid Control Systems under Grant SGJSXT00GCJS1900124.

ABSTRACT Multi-Terminal DC (MTDC) transmission systems typically operate under active power and DC voltage (P-U_{DC}) droop control for active power dispatch, and its design is greatly influenced by DC network characteristics. Hence, this paper firstly analyzes P-U_{DC} droop characteristics when implemented on Grid-Side Voltage-Source Converters (GSVSCs) of a MTDC network, in which variations of DC cables' resistances with temperature are taken into account. The analysis establishes that the actual droop characteristics of GSVSCs are nonlinear, different from the widely assumption of linear relationships. This finding is the fundamental for the design of the accurate power dispatch for GSVSCs. Therefore, an improved Fuzzy Search based Droop Control (FSDC) scheme for MTDC systems is proposed, which performs real-time search to capture the accurate droop curves of GSVSCs over full range of permissible DC voltage and active power. The FSDC is implemented without the assumption of the prior knowledge of DC network parameters which are subject to variations and uncertainty, and instead the accurate droop curves are periodically obtained and updated. The technical viability of the FSDC and its superiority over the conventional linear droop scheme under the variations of DC cable resistances and power flow variations is verified by a four-terminal HVDC model established in MATLAB/Simulink.

INDEX TERMS DC super grid, power dispatch, voltage-source converter, droop control, fuzzy search.

I. INTRODUCTION

The advancement and maturity of VSC technologies have encouraged transmission industry to develop and commission several MTDC systems in recent years, and accelerated extensive researches in the outstanding issues of the next generation of MTDC super grids [1]–[8]. VSC-MTDC systems offer several technical advantages such as:

- Lower transmission losses compared with equivalent AC systems;
- Increased flexibility of power control at VSC stations;
- Reactive power support at converter stations at no additional cost;
- Facilitating asynchronous interconnection of regional and transnational grids.

VSC-MTDC system is the preferred transmission option for connecting large-scale offshore wind farms into onshore AC grids as HVAC transmission system is inferior and suffers from high losses and poor utilization of cable cross-section in long distance applications as a result of high charging or reactive current from the cable stray capacitors [9], [10].

The planned transnational DC grid in North Sea in Europe is an example of the MTDC super grid which aims to exploit

The associate editor coordinating the review of this manuscript and approving it for publication was Tariq Masood.

and transmit the abundant wind power in North Sea to Germany, Great Britain, Norway and Belgium [5]. To ensure that the investment in this MTDC super grid is in line with offshore wind power development and does not become redundant, the planned MTDC grid is being executed to gradually increase the power transmission capacities among the countries aforementioned [6]. In recent years, China has commissioned Nan'ao four-terminal MTDC project and Zhoushan five-terminal MTDC project; however, these two projects are exploratory and built with relatively low DC voltage levels and rated powers [7]. Another planned Zhang-bei four-terminal MTDC project is rated for ±500 kV DC voltage and 6000 MW and it is expected to be completed in 2021 [8] and become a DC super grid in the real sense.

Amongst several challenges that MTDC systems face such as the absence of agreed standard (or grid code) and protection philosophies [11], ensuring an appropriate level of the DC voltage stability and accurate active power control at each VSC station represent the operational challenges to be addressed and worth of investigation. In efforts to address the abovementioned operational challenges, several studies have investigated numerous ways for controlling MTDC systems. For example, several active power and DC voltage (P-U_{DC}) droop control schemes were proposed for VSC based MTDC systems [12]–[14]. Commonly, the droop control scheme is implemented on top of the DC voltage regulator of individual VSCs and its purpose is to enable the DC voltage controlling VSC to regulate its active power output by offsetting its DC voltage. Fundamentally, the linear droop line of a given VSC is obtained by assessing the DC network electrical characteristics, particularly, the mutual equivalent DC resistances among the power-sharing VSCs.

Among the previous researches on MTDC, operation in steady state has been exhaustively explored. In [15], three different modes of DC voltage control and power dispatch of a MTDC system for integrating large offshore wind farms are discussed, under different operation conditions without taking the DC voltage drops incurred in the DC cable resistances into account. In [16], two different models are derived to research the impacts of DC line voltage drops on the power flow in MTDC, in which the relationship of P-U_{DC} is described as a linear droop interaction.

Nevertheless, as verified in the first part of this paper, the droop curve of P-U_{DC} is not strictly a linear line as usually assumed in the majority of previously published papers [1], [12]–[16]. When the VSC operates under conventional linear droop control scheme and its active power approaches the upper limit, the control error becomes significantly large. Also, the active power operating points of wind-farm VSCs (WFVSCs) influence the accuracy of the droop control scheme, which will be discussed in details later.

Furthermore, the droop coefficients are not constants as widely assumed, instead they vary as the resistances of the MTDC system cables change due to the ambient temperature variations (for offshore or onshore regions with distinct four seasons, the change in DC cable resistances over a year could be significant). Therefore, this paper suggests regular updates of the droop coefficient in effort to maintain certain degree of the control accuracy. To the authors knowledge, this issue has not been tackled yet by any paper in open literature.

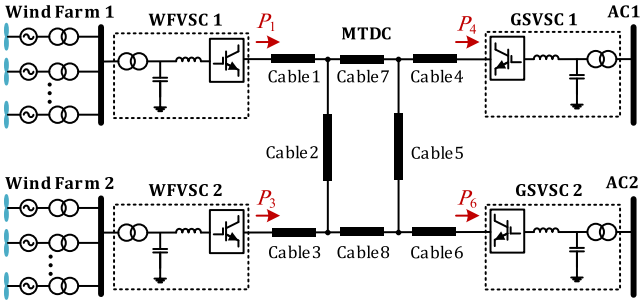

FIGURE 1. The schematic of a four-terminal HVDC transmission system.

To address the aforementioned two challenges, this paper first establishes basic P-U_{DC} characteristics using mathematical relationship that describes the steady-state behavior of a MTDC system, which initiates a more accurate design of the droop control scheme. The paper then proposes an intelligent Fuzzy Search based Droop Control (FSDC) scheme which in real-time captures the droop coefficient using fuzzy search method that is insensitive to system uncertainties and avoids any assumption on DC characteristics as well. The implementation of the proposed FSDC to the MTDC control system is also presented.

The rest of the paper is organized as follows: In section II, system configuration and conventional control modes for VSCs are introduced. In section III, the analysis on droop characteristics of P-U_{DC} is carried out as well as simulation verification. The proposed FSDC scheme is described in Section IV. Comparison & dynamic simulations with analyses are shown in Section V to validate the accuracy of the proposed FSDC scheme. The key conclusions are drawn in Section VI.

II. CONFIGURATION AND CONTROL FOR MTDC SYSTEMS

Fig. 1 displays a four-terminal HVDC system with a ring topology which consists of two WFVSC stations and two GSVSC stations. Two wind farms are integrated into the MTDC system through the two WFVSCs respectively, and the generated wind power are delivered to the two asynchronous AC grids via two separate GSVSCs.

The two WFVSCs are operated in the islanded mode, which establish and regulate the AC voltage and frequency in offshore network [17], acting as slack buses for two offshore networks respectively. The two GSVSCs are controlled under the grid-connected mode. At least one GSVSC station (in this case GSVSC1) should be assigned to regulate the DC voltage to maintain the DC voltage stability and the entire DC network power balance. The flexibility of the control objective for the other GSVSC station (in this case GSVSC2) in configuration in Fig.1 is that either it can be controlled at constant active power mode or at DC voltage regulation mode [18] as in Fig. 2.

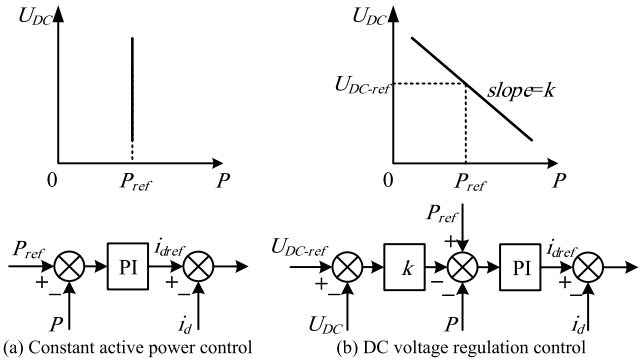

FIGURE 2. Control modes for GSVSCs.

In the case of GSVSC2 having constant active power mode, the power allocation scheme for the two GSVSCs is typically called "master and slave control", where GSVSC1 acts as the master and two WFVSCs and GSVSC2 are the slaves. However, due to the restricted DC voltage regulation capability only by GSVSC1, the MTDC system is posed with the risk of instability when GSVSC1 reaches its power limits. In such situation, the system may experience overvoltage or undervoltage problems which has adverse impacts on system components, i.e., converters and DC cables *et al*. [18].

In the case of GSVSC2 having DC voltage regulation control mode, its DC voltage reference can be offset by the active power control command. The mechanism that GSVSC2 with DC voltage regulation control mode can achieve active power control is that its terminal DC voltage errors with respect to the terminal voltage of GSVSC1 can vary the DC current exchange between the two GSVSCs. The amount of the current exchange variation is determined by the two terminal DC voltage differences and their mutual DC circuit resistances. The power allocation scheme for the two GSVSCs is normally called "Voltage Droop Control" (VDC). There have been proposals to offset both DC voltages of two GSVSCs to achieve higher level of controllability [15], but this can increase complexity and uncertainty of the control system. Therefore, in the rest of the paper, GSVSC1 is always operated at the constant DC voltage for simplicity purpose.

III. P-U_{DC} DROOP CHARACTERISTICS FOR GSVSCS

In order to analyze the P-U_{DC} droop characteristics, this section sets up a mathematical model for the MTDC system and then use the model to analyze the MTDC droop characteristics.

A. THE MTDC CIRCUIT MODEL

Fig. 3 illustrates the equivalent single-line diagram of the MTDC system as presented in Fig. 1. As for the steady-state analysis, the inductances and capacitances of the DC circuits can be neglected. R_1 to R_8 represent the DC resistances of the eight DC cables as illustrated in Fig. 1. U_1, U_3, U_4, U_6, & I_1, I_3, I_4, I_6 are the DC voltages and currents respectively at the DC terminals of the four converter stations. U_2,U_5, U_7, U_8, &

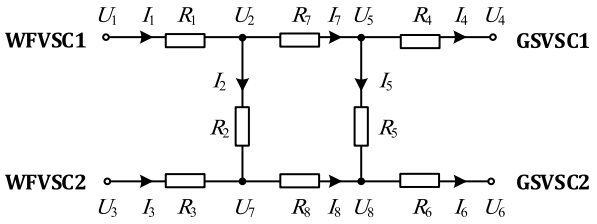

FIGURE 3. Equivalent single-line diagram of the candidate MTDC system.

I_2, I_5, I_7, I_8 refer to the DC voltages and currents respectively at the DC nodes with the locations as noted in Fig. 3.

The electrical relationship for the terminal and node currents & voltages are given by (1):

$$\begin{cases} U_1 = U_2 + R_1 I_1 \\ U_3 = U_7 + R_3 I_3 \\ U_4 = U_5 - R_4 I_4 \\ U_6 = U_8 - R_6 I_6 \end{cases} \tag{1}$$

The relationship of DC currents can be given as (2) according to Kirchhoff's Current Law:

$$\begin{cases} I_1 - I_2 - I_7 = 0 \\ I_7 - I_4 - I_5 = 0 \\ I_2 + I_3 - I_8 = 0 \\ I_5 + I_8 - I_6 = 0 \end{cases} \tag{2}$$

The DC node voltages and currents in the MTDC network are given as:

$$\begin{cases} U_2 - U_5 = R_7 I_7 \\ U_2 - U_7 = R_2 I_2 \\ U_7 - U_8 = R_8 I_8 \\ U_5 - U_8 = R_5 I_5 \end{cases} \tag{3}$$

Although GSVSC2 regulates the terminal DC voltage, the direct goal of the GSVSC2 control system under the VDC scheme is to control its active power output P_6 (or the DC current I_6). Thus, taking I_1, I_3, I_5, I_6, and U_4 as the controlled variables under the MTDC coordinated control scheme, (1) to (3) can be expressed as:

$$\begin{bmatrix} U_1 \\ U_3 \\ U_6 \\ I_4 \end{bmatrix} = \mathbf{A} \begin{bmatrix} I_1 \\ I_3 \\ I_5 \\ I_6 \\ U_4 \end{bmatrix} \tag{4}$$

where

$$A = \begin{bmatrix} R_1 + R_4 + R_7 & R_4 + R_7 & R_7 & -(R_4 + R_7) & 1 \\ R_4 & R_3 + R_4 & -(R_5 + R_8) & -R_4 + R_8 & 1 \\ R_4 & R_4 & -R_5 & -(R_4 + R_6) & 1 \\ 1 & 1 & 0 & -1 & 0 \end{bmatrix}$$

TABLE 1. Parameters of the four VSCs in MTDC system.

Terminals	P_{rated} (MW)	U_{rated} (kV)
WFVSC1	800	±400
WFVSC2	800	±400
GSVSC1	800	±400
GSVSC2	800	±400

The active power at the DC sides of the four terminals are calculated as:

$$\begin{cases} P_1 = U_1 I_1 \\ P_3 = U_3 I_3 \\ P_4 = U_4 I_4 \\ P_6 = U_6 I_6 \end{cases} \tag{5}$$

B. THE NONLINEARITY OF P-U_{DC} DROOP CHARACTERISTICS

The terminal DC voltage U_6 of GSVSC2 can be derived from (4) as in (6):

$$U_6 = R_4 I_1 + R_4 I_3 - R_5 I_5 - (R_4 + R_6) I_6 + U_4 \tag{6}$$

Based on (5) and (6), the relationship between the active power P_6 and the terminal DC voltage U_6 of GSVSC2 can be obtained as:

$$P_6 = -\frac{1}{R_6} U_6^2 + \frac{(R_4 I_4 - R_5 I_5 + U_4)}{R_6} U_6 \tag{7}$$

In consideration of the input currents from other VSCs as well as the DC circuit resistances, it is obvious from (7) that the droop characteristic of P_6-U_6 is a parabola curve rather than a linear line. In fact, once U_6 is defined at certain value by the VDC scheme, the amount of P_6 is not only related to the DC resistances R_4, R_5, and R_6 but also the current inputs I_4 and I_5 from two WFVSCs. Different active power operating points of WFVSCs result in the variations of P-U_{DC} droop characteristic for GSVSC2.

C. SIMULATION VERIFICATION OF THE NONLINEARITY OF THE DROOP CHARACTERISTICS

To illustrate that the droop characteristic of the P-U_{DC} is not linear as widely assumed in [16], a four-terminal HVDC system shown in Fig. 1 is established in MATLAB/Simulink. The simulation parameters of the MTDC are shown in Table 1.

In MTDC system simulations, all DC submarine cables are assumed to be XLPE. According to the rated DC voltage of VSCs in Table 1, DC cables 1 to 8 with ±400 kV rated voltage & 800 MVA rated power are modeled as the "π" type initially at 20 °C with parameters as presented in Table 2. The equivalent unit resistance, inductance and capacitance of the DC cables at 20 °C are respectively 0.009 Ω/km, 0.209 μF/km, and 0.5 mH/km [19]. Under real-time loads change or ambient temperatures change, the equivalent unit resistance of the DC cable changes as well, which may lead to the fluctuations of the power flow in MTDC system and the inaccuracy of DC droop coefficient. Table 3 shows corresponding DC cable resistances at 20 °C, 50 °C, and 80 °C operating temperatures, respectively [20]. In simulations, all these parameters are converted to the per-unit values with the base power of P_{base}=800 MVA and the base voltage of U_{base}=400 kV.

TABLE 2. Equivalent parameters of DC cables (at 20 °C).

Cable Number	Length (km)	Resistance (Ω)	Inductance (mH)	Capacitance (μF)
1 to 6	50	0.45	25	10.45
7 and 8	300	2.7	150	62.7

TABLE 3. Equivalent resistances of DC cables at different temperatures.

Temperature (°C)	Equivalent DC Cable Resistance (Ω/km)
20	0.009
50	0.01006
80	0.01112

To verify the derived (7) that implies the droop coefficient is a nonlinear line subject to the resistances and active power operating changes, Fig. 4 presents the simulation results in which active power and DC voltage operating points are sampled, correlated and plotted into the P-U_{DC} droop characteristics under DC cable resistances variations with the temperatures (at 20 °C, 50 °C, and 80 °C, respectively) as well as input active power from two WFVSCs. From Fig. 4(a) to 4(c), it can be observed that the droop characteristic of P_6-U_6 changes when DC resistances R_4, R_5, and R_6 vary with the temperature, which indicates that the droop characteristic of P_6-U_6 is influenced by the cable resistances as explained in (7). In Fig. 4(d), it is clear that the droop characteristic of P_6-U_6 is different when total input active power from two WFVSCs fluctuates, which entails that different active power operating points of WFVSCs have influence on the P-U_{DC} droop characteristic of GSVSC2. Especially when the active power P_6 of GSVSC2 approaches the upper limit (1 p.u.), the droop characteristic of P_6-U_6 exhibits more obvious nonlinearity as shown in the enlarged charts in Fig. 4(a) to 4(d). Operation in nonlinear sections of the droop characteristics exacerbates the inaccuracies of the active power dispatch, which cannot be avoided for the conventional VDC schemes.

To quantify the effects of the resistances R_4, R_5, and R_6 on the droop characteristic of P_6-U_6, sensitivity analysis is carried out as follows. The sensitivity of P_6 to resistances R_m ($m = 4, 5, 6$) can be defined as:

$$\alpha = \frac{\Delta P_6 / P_{base}}{\Delta R_m / R_{m-base}} \tag{8}$$

where $\Delta P_6/P_{base}$ is the percentage of the active power change and $\Delta R_m/R_{m-base}$ is the percentage of the resistances change.

Sensitivity α in (8) describes the extent at which the active power P_6 changes with the variations in the DC cable resistances as temperature varies. The bigger the sensitivity

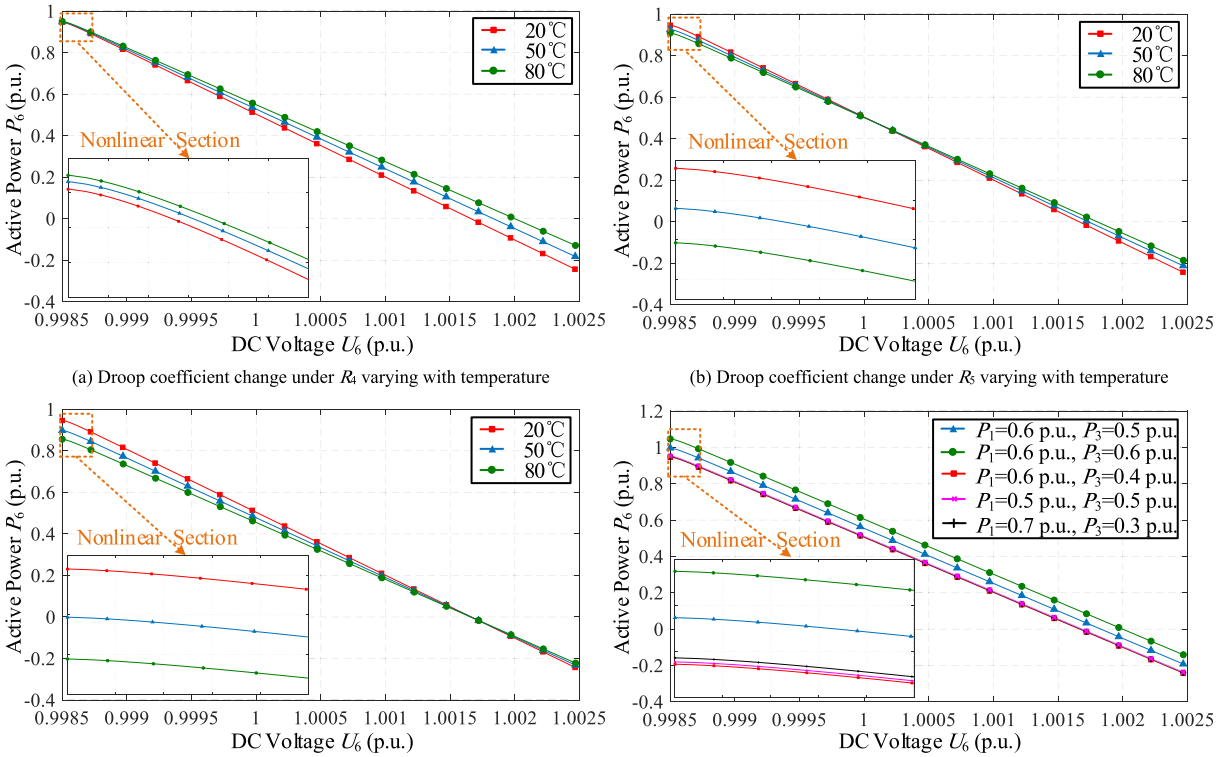

(a) Droop coefficient change under R_4 varying with temperature

(b) Droop coefficient change under R_5 varying with temperature

(c) Droop coefficient change under R_6 varying with temperature

(d) Droop coefficient change under output power from WFVSCs varying

FIGURE 4. Droop characteristics of P_6-U_6.

TABLE 4. Sensitivities of P_6 to resistances R_4, R_5, and R_6.

Variations of Resistances	R_4	R_5	R_6
-20%	0.182	0.002	0.180
-10%	0.175	0.002	0.174
0%	0	0	0
10%	0.164	0.001	0.163
20%	0.159	0.001	0.157

α is, the larger the variation of P_6 is and the more impacts the DC cable resistances have on droop characteristic of P_6-U_6. When resistances R_4, R_5, and R_6 change $\pm 10\%$ and $\pm 20\%$, respectively, the corresponding sensitivities are shown in Table 4.

From Table 4, it can be found that the impact of variations in the mutual resistance R_5 between GSVSC1 and GSVSC2 is trivial compared to the resistances R_4 and R_6.

IV. THE PROPOSED FSDC SCHEME

According to the analyses in section III, the conventional VDC scheme which applies a fixed linear P-U_{DC} droop controller may lead to the inaccuracy of the power allocation between GSVSC1 and GSVSC2. The immediate measure to avoid such an inaccuracy is to replace the conventional VDC scheme with nonlinear droop curve by (7) in considerations of DC network resistances and WFVSCs' output currents. However, the DC network resistances may vary subject to the following factors:

- Ambient environment around the cable, e.g. water or air temperature, wind speeds, solar radiations, *et al.*
- Changing in system operating points P_1 & P_3 which may cause the current in the DC cables to vary substantially.

It is worth emphasizing that it is practically challenging to accurately estimate the resistances of the DC cables in MTDC system whose length may range from tens of kilometers to hundreds of kilometers. To solve this problem, the intelligent FSDC scheme is proposed using fuzzy search.

A. FUZZY SEARCH FOR DC DROOP CHARACTERISTICS

Fig. 5 shows the proposed FSDC scheme using fuzzy search for the accurate power allocation between GSVSCs, which can be expresses as:

$$U_{DC-ref} = \begin{cases} U_{DC-\min} + \dfrac{U_{DC-\max} - U_{\text{DC-min}}}{T} \times nT_S, & S = 1 \\ U_{DC-0}, & S = 2 \end{cases} \tag{9}$$

where $U_{\text{DC}-\min}$ and $U_{\text{DC}-\max}$ refer to the minimum and maximum operational range of the DC voltage respectively. T refers to the total control time of the FSDC, T_S refers to the sampling period of the control, and $n = 1, 2, 3 \ldots S$

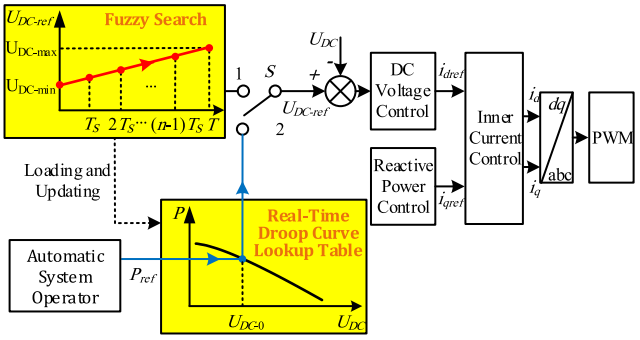

FIGURE 5. Framework of FSDC scheme.

denotes the operating state of the fuzzy search (when S=1, fuzzy search in Fig.5 is switched on; when S=2, switched off), and U_{DC-0} refers to the corresponding reference DC voltage with respect to the active power command as loaded from the fuzzy search.

As illustrated in Fig. 5, when S switches to the position 1 (S=1), fuzzy search method is switched on for GSVSC2 to scan for the correct droop curve of P_6-U_6. The fuzzy search captures the droop curve in real time by controlling GSVSC2 DC voltage from U_{DC-min} to U_{DC-max} and in the meanwhile recording the corresponding active power operating points. When fuzzy search is completed at T, the array of (P_{6i}, U_{6i}) (i=1, 2, 3 …n) are obtained. For capturing more accurate droop curve of P_6-U_6, T could be larger and T_S smaller to collect (P_{6i}, U_{6i}) as much as the real operation permits. Then the discrete nonlinear droop curve data points (P_{6i}, U_{6i}) can be fitted to a continuous line of P_6-U_6 using the Least Squares method [21], [22] as follows.

Equation (7) can be rewritten to facilitate the data manipulation as follows:

$$P_6 = kU_6^2 + bU_6 \tag{10}$$

where both k and b are the coefficients of the nonlinear droop curve.

According to the Least Squares method, the best curve-fitting $f_{LS}(k, b)$ are achieved by minimizing the sum of the squared residuals between the observed values of (P_{6i}, U_{6i}) and the fitted values provided by the assumed model in (10), which is expressed as:

$$f_{LS}(k, b) = \min(\sum_{i=1}^{n} (kU_{6i}^2 + bU_{6i} - P_{6i})^2) \tag{11}$$

With collected (P_{6i}, U_{6i}), the corresponding droop curve coefficients k and b of the best droop-curve-fitting in (10) can be calculated by (11) so that the real-time droop characteristic of P_6-U_6 is obtained.

B. REAL-TIME DROOP CURVE LOOKUP TABLE

After fuzzy search is completed, the real-time droop curve P_6-U_6 is updated and loaded to the real-time droop curve lookup table as illustrated in Fig. 5. To adopt the updated

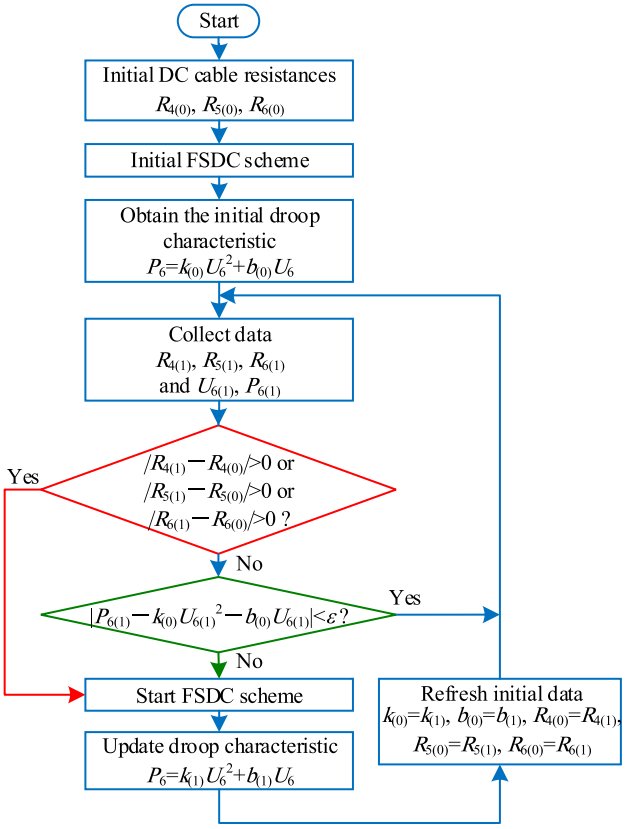

FIGURE 6. Droop coefficients capture process in the FSDC scheme.

droop curve, S switches to the position 2 (S=2). With the real-time droop curve lookup table, the active power set-point (P_{ref}) from the automatic system operator checks the real-time droop curve lookup table to define the GSVSC2 DC voltage reference value U_{DC-0}. Automatic system operator can set any P_{ref} for dispatch purpose and the fuzzy search process & the updated droop curve lookup table ensures the control accuracy for the closest time beings.

C. PERIODICAL UPDATE OF THE DROOP CURVE

The process of the periodical update of the droop curve in FSDC scheme is illustrated in the flowchart of Fig.6. In Fig. 6, all variables with subscript 0 are corresponding initial values while with subscript 1 are values at next time of data collection. To timely acquire and update the correct droop curve of P_6-U_6 whose accuracy is subject to the DC network resistance changes and input active power changes, online estimation of droop coefficients in (10) has to be carried out periodically using the criterion as shown in Fig. 6.

The real-time droop coefficients $k_{(0)}$ and $b_{(0)}$ are calculated starting from an initial droop curve of P_6-U_6 assuming fixed operating condition and initial resistances $R_{4(0)}$, $R_{5(0)}$, and $R_{6(0)}$. If the estimated DC cable resistances at next time (as represented as $R_{4(1)}$, $R_{5(1)}$, and $R_{6(1)}$ in Fig.6) or total input active power from WFVSCs are judged unchanged, the initial droop curve of P_6-U_6 stored in real-time droop curve lookup

table as shown in Fig. 5 is kept unchanged and the active power dispatch for GSVSC1 and GSVSC2 remains precise.

The first criterion to trigger FSDC scheme is identified by (12):

$$\left|R_{4(1)}-R_{4(0)}\right|>0 \; or \; \left|R_{5(1)}-R_{5(0)}\right|>0 \; or \; \left|R_{6(1)}-R_{6(0)}\right|>0 \tag{12}$$

With (12), once any of the estimated resistances at next time point differs from the initial values, the resistance variations with the ambient temperature or load currents are fed to the FSDC scheme. S is then immediately switched by the FSDC scheme to the position 1 and the real-time capturing of the droop characteristics P_6-U_6 using fuzzy search starts. Through the fuzzy search process, the droop curve of P_6-U_6 in real time with new coefficients of $k_{(1)}$ and $b_{(1)}$ is obtained and then it is updated to the real-time droop curve lookup table. After the fuzzy search and the recording are completed, S is switched to position 2 again.

The second criterion to trigger the FSDC scheme is the fluctuations of the MTDC input active power which also influences the accuracy of the droop characteristics. The detection criterion is expressed by:

$$\left|P_{6(1)}-k_{(0)}U_{6(1)}^2-b_{(0)}U_{6(1)}\right|<\varepsilon \tag{13}$$

where ε represents an infinitesimal constant near to zero.

If $|P_{6(1)}-k_{(0)}U_{6(1)}^2-b_{(0)}U_{6(1)}|$ is smaller than ε, there is no need to start fuzzy search to update the droop curve and the operating point of GSVSC2 at next time point remains on the initial droop curve. Nevertheless, $|P_{6(1)}-k_{(0)}U_{6(1)}^2-b_{(0)}U_{6(1)}|>\varepsilon$, indicates a considerable change of the MTDC system power flows, so that the fuzzy search will start to capture the new droop curve and update it into the real-time droop curve lookup table. After the update of droop curve, initial data is refreshed for the power dispatch at a future time point.

In brief, to ensure the active power control accuracy for GSVSCs, the proposed FSDC scheme updates the droop curve in real time on detections of the variations of DC cable resistances and the input active power flows.

Fig. 7 presents the real-time fuzzy search process where DC voltage level of GSVSC2 is controlled to vary and result in active power relocations between GSVSC1 and GSVSC2. The fuzzy search period T is set to 15 s of a substantially long period in order to avoid transient intervention from the VSC high-bandwidth controllers. The data array (P_{6i}, U_{6i}) of the droop characteristics is obtained by the fuzzy search control block as described by (9), (10) and (11) and loaded to the droop curve lookup table as illustrated in Fig.5.

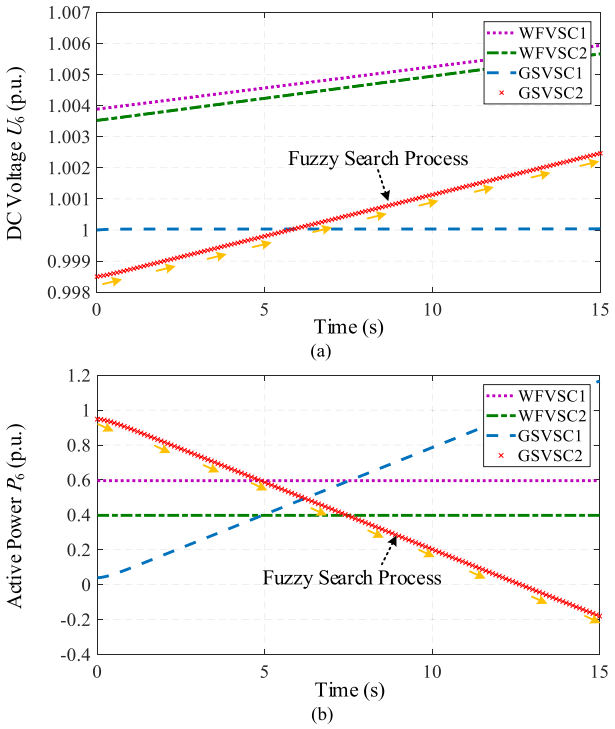

FIGURE 7. Dynamic responses of the fuzzy search in FSDC scheme.

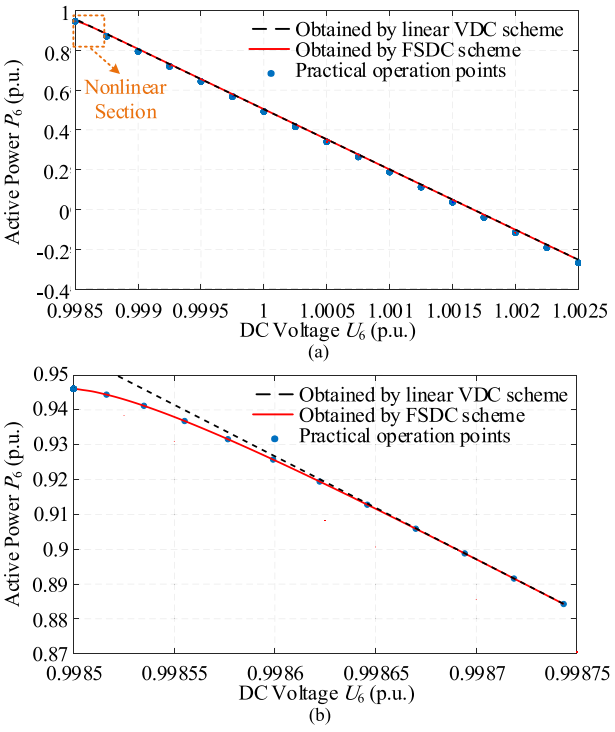

FIGURE 8. Comparison of droop curves between FSDC scheme and conventional linear VDC scheme.

V. ACCURACY VERIFICATION OF FSDC SCHEME

To verify the accuracy of the proposed FSDC scheme over the conventional linear VDC scheme for active power dispatch, simulation comparisons between the two control schemes are carried out in this section. The simulation model is the same as the one described in Section III.

A. COMPARISON OF DROOP CURVE

Both the proposed FSDC scheme and the conventional VDC scheme obtains their droop characteristics at the same GSVSC2 DC voltage references ranging from 0.9985 p.u. to 1.0025 p.u. at the cable temperature 20 °C as shown in Fig.8.

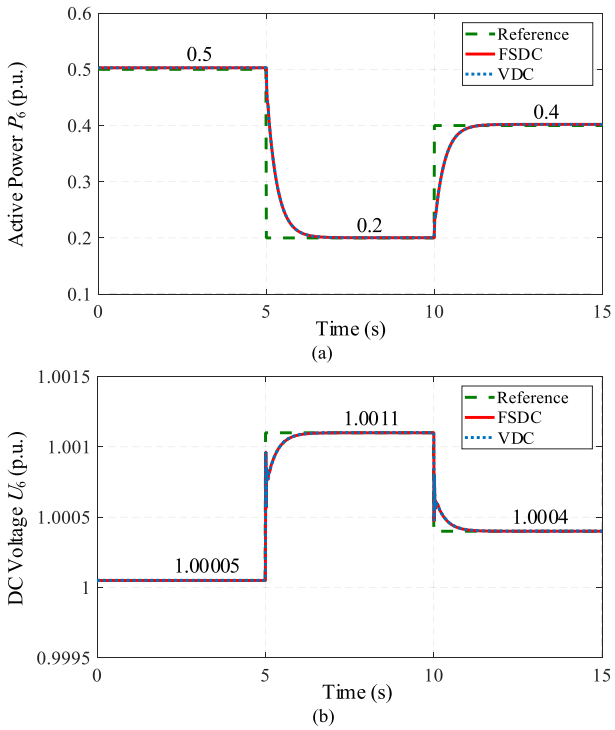

FIGURE 9. Step responses of GSVSC2 in linear section.

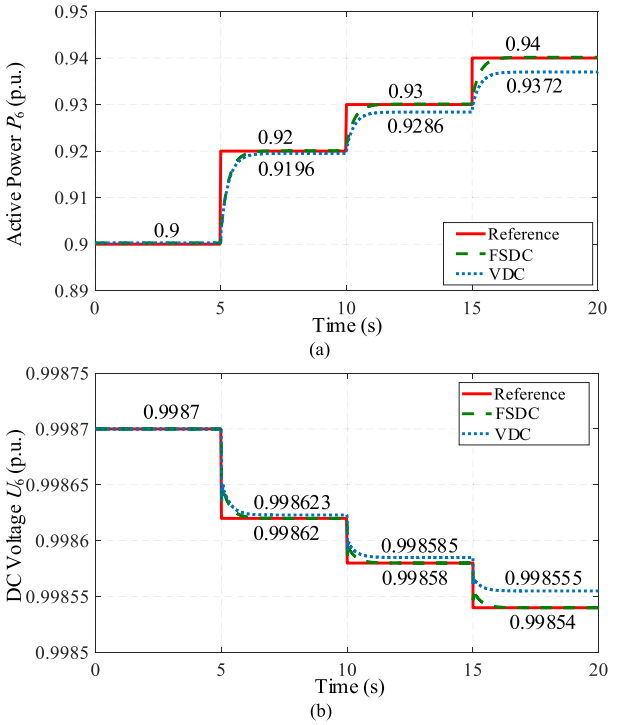

FIGURE 10. Step responses of GSVSC2 in nonlinear section.

As observed from Fig. 8(a) that when the DC voltage is varied, the operational droop characteristics under the proposed FSDC scheme as drawn in red solid lines is proved to be generally in the same overall trend with the droop characteristics under the conventional linear VDC scheme as signified by black dotted line. In the droop linear section from 0.99875 p.u. to 1.0025 p.u. of the DC voltage levels, both droop curves of P_6-U_6 from the two schemes are identical and therefore the active power dispatch for the GSVSCs are accurate for the conventional VDC scheme.

However, when the DC voltage varies from 0.9985 p.u. to 0.99875 p.u. as shown in enlarged chart in Fig. 8(b), as analyzed by (7), errors between the droop curves of the conventional VDC scheme in black dotted line and the corrected droop curve in red solid line increase, which is further verified through the actual operation points as presented in blue dots by the simulation. This simulation result proves the accuracy of the proposed FSDC scheme compared to the conventional linear VDC scheme.

B. COMPARISON OF STEP DYNAMIC RESPONSES

Fig. 9 and Fig. 10 show the time-domain GSVSC2 dynamic responses under the proposed FSDC scheme and the conventional linear VDC scheme to the active power reference step changes. It can be seen from Fig.9, for the droop linear section (P_{ref} ranging from 0.5 p.u. to 0.2 p.u. then to 0.4 p.u. at times t=5 s and 10 s respectively) that both schemes can precisely achieve the active power tracking.

In contrast, as observed from Fig.10 for the droop nonlinear section (P_{ref} from 0.9 p.u. to 0.92 p.u. to 0.93 p.u. and then to 0.94 p.u. at times t=5 s, 10 s and 15 s respectively) it is evident that the FSDC scheme is superior over the conventional VDC scheme as the apparent errors between the active power reference and the actual active power settled points are observed in the VDC GSVSC2 responses. Moreover, the error is as predicted by (7) and Fig.8(b) increasingly large when the GSVSC2 active power approaches its 1 p.u. power limit.

The proposed FSDC scheme can successfully guarantee the precision of the active power dispatch for the GSVSC1. It is also worth noticing that as discussed in Fig. 4, the droop curve can be significantly deviated from the predefined droop line by the VDC scheme, causing large active power control errors; therefore it is necessary to periodically update the droop curves according to the criteria as defined in (12) and (13) by the proposed FSDC scheme.

VI. CONCLUSION

An improved fuzzy search based droop control (FSDC) scheme for the accurate power dispatch of GSVSCs in MTDC transmission systems has been proposed in this paper. This paper firstly derives an accurate mathematical model of the droop coefficients. Using this model, the analysis of P-U_{DC} droop characteristics of GSVSC in a MTDC system has revealed that the "hidden" nonlinearity is introduced as system parameters and operating temperatures vary, and this nonlinearity is exacerbated especially when the GSVSC approaches its active power limit. The emergence of this nonlinearity is further verified by the time-domain simulations,

and it is deemed to degrade the performance of the widely accepted linear droop control scheme in terms of accuracy of the power dispatch in MTDC system. Then this paper proposes a fuzzy search process to capture the precise droop coefficients through real-time operating points using the Least Squares method and load the coefficients into the real-time droop curve lookup table for active power dispatch. The criteria to trigger the proposed FSDC scheme for updating the droop coefficients are elaborately designed to detect the operational condition changes.

Exhaustive comparative studies have shown that the proposed FSDC scheme is superior to the conventional linear droop scheme in tracking accuracy of the power set-points and dynamic responses. Besides the accuracy, it is scalable to the MTDC transmission system with large number of converter terminals, benefiting from powerful fuzzy search techniques and ease of implementation that avoid complex computations of MTDC network characteristics.

REFERENCES

[1] S. Song and L. Sun, "Research on the internal modal decoupling control of VSC-MTDC," *J. Eng.*, vol. 16, no. 3, pp. 3359–3364, Apr. 2019.

[2] W. Wang, Y. Li, Y. Cao, U. Häger, and C. Rehtanz, "Adaptive droop control of VSC-MTDC system for frequency support and power sharing," *IEEE Trans. Power Syst.*, vol. 33, no. 2, pp. 1264–1274, Mar. 2018.

[3] Z.-D. Wang, K.-J. Li, J.-G. Ren, L.-J. Sun, J.-G. Zhao, Y.-L. Liang, W.-J. Lee, Z.-H. Ding, and Y. Sun, "A coordination control strategy of voltage-source-converter-based MTDC for offshore wind farms," *IEEE Trans. Ind. Appl.*, vol. 51, no. 4, pp. 2743–2752, Jul./Aug. 2015.

[4] J. Lei, T. An, Z. Du, and Z. Yuan, "A general unified AC/DC power flow algorithm with MTDC," *IEEE Trans. Power Syst.*, vol. 32, no. 4, pp. 2837–2846, Jul. 2017.

[5] Authority of the House of Commons, London, U.K. (Sep. 2011). *A European Supergrid*. [Online]. Available: https://publications.parliament.uk/pa/cm201012/cmselect/cmenergy/1040/1040.pdf

[6] Nationalgrid, U.K. (Jul. 2017). *Network Options Assessment for Interconnectors*. [Online]. Available: https://www.nationalgrid.com/sites/default/files/documents/NOA%20for%20IC%20methodology%20final.pdf

[7] G. Buigues, V. Valverde, and A. Etxegarai, "Present and future multiterminal HVDC systems: Current status and forthcoming developments," in *Proc. ICREPQ Conf.*, Málaga, Spain, Apr. 2017.

[8] State Grid Corporation of China. *C-EPRI, Zhang-Bei DC Grid Pilot Project*. Accessed: Feb. 28, 2018. [Online]. Available: http://www.cepri.com.cn/

[9] C. Li, P. Zhan, J. Wen, M. Yao, N. Li, and W.-J. Lee, "Offshore wind farm integration and frequency support control utilizing hybrid multiterminal HVDC transmission," *IEEE Trans. Ind. Appl.*, vol. 50, no. 4, pp. 2788–2797, Jul./Aug. 2014.

[10] K. Sun, K.-J. Li, W.-J. Lee, Z.-D. Wang, W. Bao, Z. Liu, and M. Wang, "VSC-MTDC system integrating offshore wind farms based optimal distribution method for financial improvement on wind producers," *IEEE Trans. Ind. Appl.*, vol. 55, no. 3, pp. 2232–2240, May/Jun. 2019.

[11] D. Van Hertem and M. Ghandhari, "Multi-terminal VSC HVDC for the European supergrid: Obstacles," *Renew. Sustain. Energy Rev.*, vol. 14, no. 9, pp. 3156–3163, Dec. 2010.

[12] A. Thoen, M. Svean, O. Lebas, R. Irnawan, and F. F. da Silva, "Droop control optimization for multi-terminal HVDC transmission system," in *Proc. 53rd UPEC*, Glasgow, U.K., Sep. 2018.

[13] K. Rouzbehi, A. Miranian, J. I. Candela, A. Luna, and P. Rodriguez, "A generalized voltage droop strategy for control of multiterminal DC grids," *IEEE Trans. Ind. Appl.*, vol. 51, no. 1, pp. 607–618, Jan./Feb. 2015.

[14] W. Wang and M. Barnes, "Power flow algorithms for multi-terminal VSC-HVDC with droop control," *IEEE Trans. Power Syst.*, vol. 29, no. 4, pp. 1721–1730, Jul. 2014.

[15] L. Xu and L. Yao, "DC voltage control and power dispatch of a multi-terminal HVDC system for integrating large offshore wind farms," *IET Renew. Power Gener.*, vol. 5, no. 3, pp. 223–233, May 2011.

[16] T. M. Haileselassie and K. Uhlen, "Impact of DC line voltage drops on power flow of MTDC using droop control," *IEEE Trans. Power Syst.*, vol. 27, no. 3, pp. 1441–1449, Aug. 2012.

[17] J. Zhu, M. J. M. Guerrero, W. Hung, C. D. Booth, and G. P. Adam, "Generic inertia emulation controller for multi-terminal voltage-source-converter high voltage direct current systems," *IET Renew. Power Gener.*, vol. 8, no. 7, pp. 740–748, Sep. 2014.

[18] J. Zhu, C. D. Booth, G. P. Adam, and A. J. Roscoe, "Coordinated direct current matching control strategy for multi-terminal DC transmission systems with integrated wind farms," *Electr. Power Syst. Res.*, vol. 124, pp. 55–64, Jul. 2015.

[19] *230/400 kV XLPE Insulated, PE Sheathed High Voltage Power Cables*. [Online]. Available: http://www.caledoniancable.com/English/product/hv/400kv.html

[20] P. De Bruyne and B. Currat, "Temperature and frequency effects on cable resistance," AESA Cortaillod, Switzerland, Tech. Rep. AN1506A, 2015. [Online]. Available: https://www.aesa-cortaillod.com/fileadmin/documents/knowledge/AN_150617_E_Snapshots_multimaterials.pdf

[21] K. Levenberg, "A method for the solution of certain non-linear problems in least squares," *Quart. Appl. Math.*, vol. 2, pp. 164–168, Feb. 1944.

[22] G. Golub and V. Pereyra, "Separable nonlinear least squares: The variable projection method and its applications," *Inverse Problems*, vol. 19, no. 2, pp. R1–R26, Apr. 2003.

JIEBEI ZHU (M'13) received the B.S. degree in microelectronics from Nankai University, Tianjin, China, in 2008, and the M.S. and Ph.D. degrees in electronic and electrical engineering from the University of Strathclyde, Glasgow, U.K., in 2009 and 2013, respectively.

He is currently a Professor with the School of Electrical and Information Engineering, Tianjin University. From 2013 to 2018, he acted as a Senior Power System Engineer and the Innovation Project Manager with National Grid Plc. of the GB transmission system operator. His research interests involve with HVDC transmission system control, renewable energy systems, and energy storage technologies.

Dr. Zhu was awarded with the license of Chartered Engineer by U.K. Engineering Council and IET.

FENG LI was born in Shanxi, China, in 1993. She received the B.S. and M.S. degrees in electrical engineering from the Taiyuan University of Technology, Shanxi, in 2016 and 2019, respectively. She is currently pursuing the Ph.D. degree in electrical engineering with Tianjin University, Tianjin, China. Her current research interests include control strategy of power dispatch for MTDC systems and control strategy for voltage-source converters.

YINGSHU LIU was born in 1971. He received the B.S. and M.S. degrees from Zhejiang University, Zhejiang, China, in 1993 and 1996, respectively, and the Ph.D. degree from Tianjin University, Tianjin, China, in 1999.

He is currently an Associate Professor with the School of Electrical and Information Engineering, Tianjin University. His research interests include operation control strategy and energy management of microgrid, the energy Internet, and energy router and implementations of control and communication technologies in smart grid.

GRAIN PHILIP ADAM (M'12) received the B.S. and M.S. degrees (Hons.) from the Sudan University for Science and Technology, in 1998 and 2002, respectively, and the Ph.D. degree in power electronics from the University of Strathclyde, Glasgow, U.K., in 2007.

He has been a Researcher with the University of Strathclyde, since 2008. His research interests are fault tolerant voltage source converters for HVDC applications, modeling and control of HVDC transmission systems and multiterminal HVDC networks, voltage-source-converter-based FACTS devices, and grid integration issues of renewable energies.

Dr. Adam is also an Active Contributor to reviewing process for several IEEE and IET Transactions, journals, and conferences. He is also an Associate Editor of the *Journal of Emerging and Selected Topics in Power Electronics*.

MINGYING LI is currently an Engineer with the State Grid Electric Power Research Institute, Nanjing, China. His main research field is power system stability control.

NING SUN is currently an Engineer with the State Grid Electric Power Research Institute, Nanjing, China. His main research field is power system stability control.